MAGNETIC FIELD EVOLUTION OF AR 0486 BEFORE AND AFTER THE X17 FLARE ON OCTOBER 28, 2003

S. Régnier and B. Fleck

ESA Research and Scientific Support Department, ESTEC, 2200 AG Noordwijk, The Netherlands

ABSTRACT

Over two weeks in October/November 2003, the Sun featured unusually strong activity, with three large sunspot groups (including the largest one of this solar cycle), twelve X-class flares (including the strongest ever recorded), numerous halo coronal mass ejections (two with near-record speeds) and two significant proton storms. Eight of the twelve X-class flares originated from active region AR 10486. In this paper we investigate the coronal magnetic field configuration of AR 10486 and its time evolution around the X17.2 flare on October 28. We use two different methods. The first method is to compute the potential field from SOHO/MDI line-of-sight magnetograms and then to derive the magnetic energy in the coronal volume and to examine the changes in the geometry of the magnetic field. We did not detect any significant change in the magnetic configuration before and after the flare. The magnetic energy follows the evolution of the photospheric unsigned magnetic flux. The second method is to determine the nonlinear force-free (*nlff*) field from one vector magnetogram (IVM/MSO). From that we obtain a better description of the geometry and topology of the magnetic field. At the location of the flare, the magnetic configuration exhibits a null point (or a separator field line in 3D) with reversed-Y shape. We estimate the free magnetic energy budget to be 5 10^{32} erg which represents only 7% of the *nlff* magnetic energy.

Key words: Sun:corona; magnetic fields; flares.

1. INTRODUCTION

The coronal magnetic field determines the coronal structure and dynamics from the upper chromosphere out into the heliosphere and is the key driver of solar eruptive events. Unfortunately, direct measurements of the coronal magnetic field are extremely difficult and it is only recently that first Zeeman splitting observations of infrared coronal emission lines have been successfully used to determine the line-of-sight magnetic flux density and transverse field orientation above an active region in the corona (Lin et al. 2004). Therefore other technics have been developed. The most promising is the extrapolation into the corona of the photospheric magnetic field which can be easily measured. This method assumes that the coronal magnetic configuration is in a magnetostatic equilibrium ($\vec{j} \wedge \vec{B} = \vec{0}$) at the time of observation. Three kinds of equilibria can be defined: the potential field ($\vec{j} = \vec{0}$), the linear and the nonlinear force-free field ($\vec{j} = \alpha \vec{B}$ where α is a constant inside the coronal volume or a function of the position). The magnetic energy of the potential field configuration (E_{pot}) is the lowest magnetic energy (E_m) a magnetic configuration can reach with the same photospheric field. To date the most realistic model is the nonlinear force-free (*nlff*) model which requires the knowledge of the photospheric magnetic field vector. Even if the physical meaning of a potential configuration is poor, the computation is fast and only requires the line-of-sight (LOS) photospheric magnetic field which is currently provided on a "real-time" basis. We investigate the relevant information that we can retrieve from the potential field extrapolations.

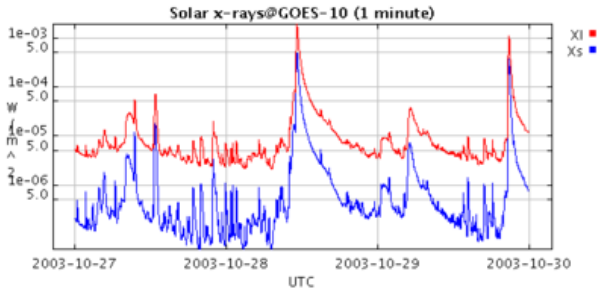

Figure 1. Solar X-ray flux observed by GOES-10 from Oct 27 to Oct 29, 2003 (graph produced by SPIDR).

In the framework of space weather, we need new methods that allow us to extract useful information from observations quickly and reliably. In this paper, we propose a new method to follow the dynamics of the coronal magnetic field as potential field extrapolated from photospheric LOS magnetograms and we compare that with the *nlff* field. In Section 3., we detail the SOHO/MDI observations and the IVM/MSO vector magnetograms used in this study. In Section 4., we study the time evolution of AR 0486 before and after the X-class flare as deduced from the potential field extrapolations, and in Section 5 we present results from our nonlinear force-free modelling, which give a more accurate description of the coronal field involved in the eruptive process.

2. FLARING ACTIVE REGION 10486

We first look at the solar X-ray flux as observed by GOES-10 close to the Earth (Fig. 1). The plot shows the X-ray flux from Oct 27 to Oct 29, 2003, integrated in the wavelength range 1–8 Å (red curve) and 0.5–4 Å (blue curve). An X17.2 flare was recorded on Oct 28 with a peak intensity at 11:10 UT. This flare originate in AR 0486 as observed by the Extreme ultraviolet Imaging Telescope (EIT) on board SOHO. The flare was associ-

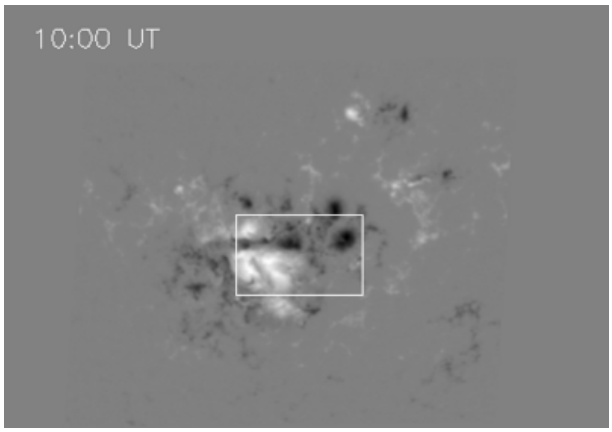

Figure 2. Vertical magnetic field of AR 0486 as observed by SOHO/MDI on October 28, 2003 at 10:00 UT. The field-of-view is 850"×600", the spatial resolution is 1.97". The white rectangle is the field-of-view used in Fig. 3.

ated with an Earth-directed CME.

3. MAGNETIC DATA

3.1 MDI

In order to follow the magnetic field evolution, we use 96 min LOS magnetograms from Oct. 27 to Oct. 29 as well as 1 min cadence LOS magnetograms including the flare period from 10:00 UT to 12:50 UT on Oct. 28. For each time series, we transform the LOS magnetograms into vertical magnetograms in the disk-center heliographic coordinate frame. This assumes that the observed magnetic field is essentially vertical on the photosphere. The time series are cross-correlated to ensure that the coronal volume is the same for each magnetogram. Fig. 2 shows the distribution of the vertical magnetic field on the photosphere at 10:00 UT on Oct 28, 2003 in a field-of-view of 850"×600". We note the complex distribution of the field with mixing polarities and sunspots with magnetic field strengths over 2500 G. The site of the flare is above the negative polarity that is oriented East-West and divides the positive polarities into a North and a South polarity (inside the rectangle).

The 96 min time series allows us to look at the long-term evolution of AR 0486. From Oct 27 to Oct 29, the main magnetic field changes on the photosphere are the emergence of two dipolar regions on the North-West side of AR0486.

The 1 min time series is useful to study the response of the magnetic field to the flare. We especially focus on the time period between 11:01 UT and 11:15 UT which corresponds to the start time of the flare and the end time of photospheric changes. In Fig. 3, we show a series of magnetograms of the region where the X-class flare occurred. From left to right and top to bottom, we have the 1 min cadence magnetograms between 11:01 UT and

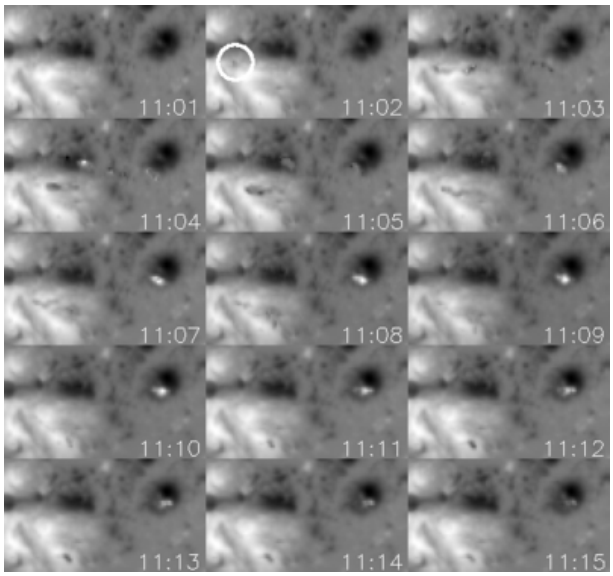

Figure 3. Time series of 1 min cadence MDI magnetograms showing the evolution of the vertical magnetic field during the X-class flare from 11:01 UT to 11:15 UT on Oct 28, 2003. The circle indicates the location of the first appearance of the "parasitic" polarity.

11:15 UT with a field-of-view of 190"×120". The flare starts at 11:02 UT (first row, second column). At that time we observe the appearance of a "parasitic" negative polarity (circle). This polarity moves to the West and is associated with a conjugate footpoint appearing as a parasitic positive polarity embedded in the negative polarity. These footpoints are moving inside the sunspot. These parasitic polarities, however, are unphysical and therefore not real. They are induced by the instrument reponse due to the disturbances created by the flare (extremely high Doppler shifts of the NiI line). As a result, the unsigned magnetic flux decreases between 11:05 UT and 11:08 UT, followed by an increase after the disturbance has disappeared. These changes, however, are not real, as they are a result of these unphysical "parasitic" polarities.

3.2 IVM

To determine the coronal magnetic field as a *nlff* equilibrium, we need the three components of the magnetic field on the photosphere. For AR 0486, there was good coverage, especially by the Imaging Vector Magnetograph at Mees Solar Observatory (IVM, Mickey et al. 1996, Labonte et al. 1999) and by the Solar Magnetic Field Telescope at Huairou Solar Observing Station (SFMT). Here we compute the *nlff* for AR 0486 observed by IVM on October 27 at 18:36 UT with a nominal spatial resolution of 0.56" and a field-of-view of 280"×180". As for the MDI magnetograms, we transform the observed magnetic field components into a disk-center heliographic frame given the three components, (B_x, B_y, B_z). The error on the measurement is estimated to be 50 G for the vertical component and 150 G for the transverse field.

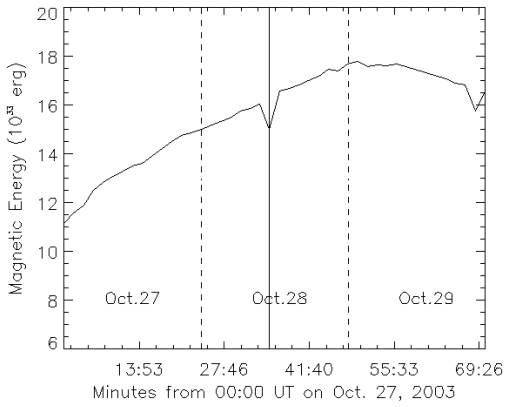

Figure 4. Magnetic energy in the corona above AR 0486 using a time series of 96 min cadence MDI magnetograms from Oct 27 to Oct 29. The dashed vertical lines separate the different days. The solid line indicates the flare time.(unit of 10^{33} erg)

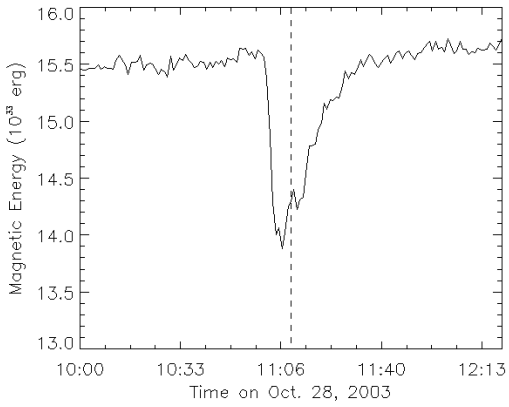

Figure 5. Same as Fig. 4 using 1 min cadence MDI magnetograms on Oct 28 from 10:00 UT to 12:20 UT. The dashed line is the time of the intensity peak observed by GOES-10.(unit of 10^{33} erg)

4. POTENTIAL FIELD

We compute the potential magnetic field into the corona from both the 96 min and the 1 min time series. From these extrapolations we derive the magnetic energy, E_m, inside the coronal volume Ω:

$$E_m = \int_\Omega \frac{B^2}{8\pi}\, d\Omega \qquad (1)$$

In Fig. 4, we plot E_m as a function of time between Oct 27 and Oct 29. The magnetic energy of the potential field is larger than 10^{34} erg due to high photospheric magnetic field strength (> 2500 G). We note that the magnetic energy increases by a factor of 1.6 between 00:00 UT on Oct 27 and $\sim$4:00 UT on Oct 29 before it decreases until the end of the time series. As the active region was crossing the central meridien on Oct 29 around 18:00 UT, we can conclude that this flux increase is related to the emergence of new flux (the two North-West dipoles), and not related to a projection effect. We also notice that a decrease of magnetic energy is observed at the time of the flare (solid line in Fig. 4). To check if this energy drop is real, we follow the evolution of the magnetic energy around the flare time using the high cadence (1 min) magnetograms. In Fig. 5 we plot E_m between 10:00 UT and 12:20 UT. We again observe the energy drop when the flare starts (11:02 UT) until 11:06 UT, followed by a rapid increase until 11:25 UT after which it reaches the same energy value as before the flare. The magnetic energy of the potential field follows the same evolution as the unsigned photospheric magnetic flux in the field-of-view of Fig. 3. The decrease and increase in magnetic energy is due to the parasitic polarity mentioned above, and therefore not real.

We now investigate the evolution of the potential field magnetic configuration of AR 0486 before, during and after the flare period. We did not observe any obvious changes in the coronal magnetic configuration of AR 0486. The photospheric changes described above imply small-scale changes in the magnetic field configuration (< 5Mm) but the large scale potential field is not modified before, during and after the flare. In Fig. 6, the magnetic configuration before the flare exhibits a system of loops (red field lines), the footpoints of which are associated with the "parasitic" polarities observed by MDI (see Fig. 3). We speculate that the "parasitic" signal is a result of flare induced disturbances that propagated along the loops and impinged on the photosphere at the footpoints

5. NONLINEAR FORCE-FREE CONFIGURATION

The *nlff* field is computed using the vector potential Grad-Rubin-like method (Amari et al. 1997; Amari et al. 1999; Régnier et al. 2002). As photospheric boundary condition, we use one vector magnetogram observed by IVM on Oct. 27 at 18:36 UT. The boundary conditions on the other sides of the box are $\vec{B} \cdot \vec{n} = 0$. This means that no field line can leave or enter the box.

In Fig. 7, we plot only a few field lines which characterize the magnetic field configuration close to the flare site. On the left is a top view of the entire field-of-view used to determine the *nlff* field (280"$\times$180"). The vertical magnetic field component is drawn as the background image as well as contours (solid contours for the positive polarities and dashed contours for the negative polarities). On the right, we have a close-up top view of the flare site as well as a side view of the magnetic configuration. We can see that the topology of the field exhibits a reversed-Y-type null point (or separator in 3D).

We derive the potential field magnetic energy, $E_{pot} = 6.5\ 10^{33}$ erg, the magnetic energy of the nonlinear force-free field, $E_{nlff} = 7\ 10^{33}$ erg. Therefore the free energy budget ($E_{nlff} - E_{pot}$) inside the magnetic configuration is of $5\ 10^{32}$ erg (7% of E_{nlff}).

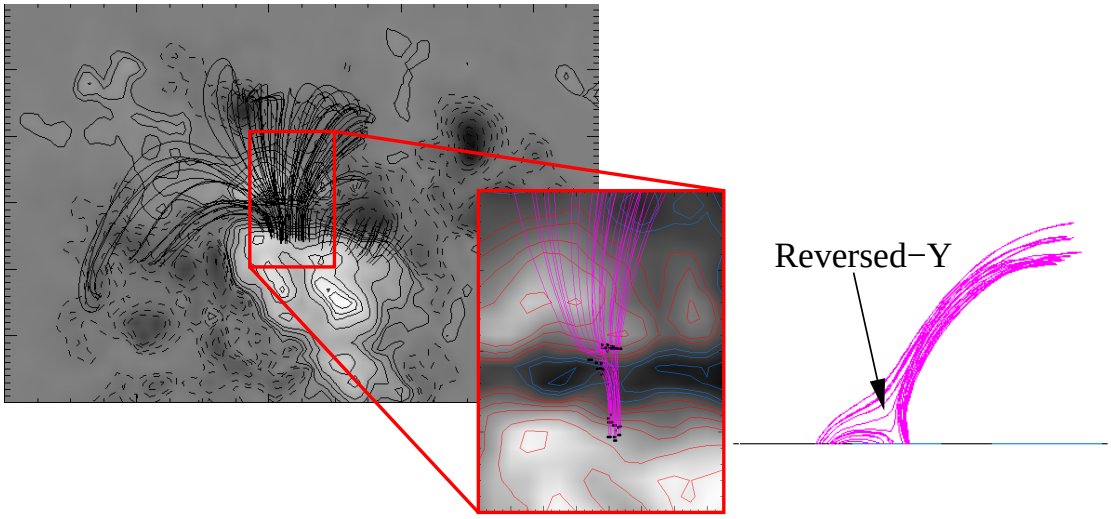

Figure 7. Nonlinear force-free configuration of AR 0486 at 18:36 UT on Oct. 27 (left image) with the IVM vertical magnetic field as background image and as contours (solid contours: positive polarities, dashed contours: negative polarities). We focus on the field lines close to the location of the flare (right images) with a top view and a side view of the magnetic configuration (see text for detail).

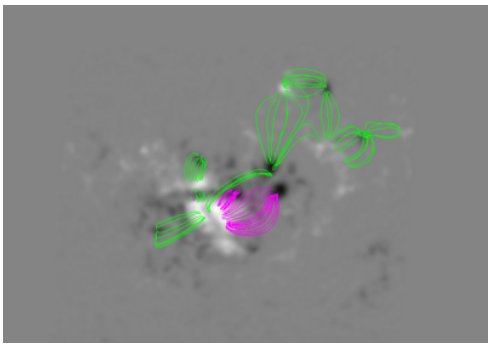

Figure 6. Potential magnetic field configuration of AR 0486 at 10:00 UT on Oct. 28. The red field lines indicate the location of the flare disturbance. The green field lines show the global topology of the active region.

6. DISCUSSION AND CONCLUSIONS

Using two different methods, we have studied the magnetic field configuration of AR 10486 before, during, and after the X17.2 flare on October 28, 2003. The first method is to determine the coronal potential field from line-of-sight photospheric measurements. Using that method we followed the time evolution of the magnetic energy and possible changes in the magnetic configuration. The advantages of this method are: line-of-sight magnetograms can be easily produced with a high spatial and high time resolution, the potential field extrapolations are fast and can be easily implemented on any computer. Therefore this method can be readily used for space weather applications. A (serious) disadvantage is that the potential field is most of the time not a realistic approximation for active region magnetic fields. The second method is to reconstruct a snapshot of the active region with a nonlinear force-free model. This method uses a photospheric vector magnetic field measurement. As we take into account the localized electric currents inside the magnetic configuration, the determination of the magnetic field is more accurate. But the *nlff* computation is time consuming.

For the X-class flare which occurred in AR 0486, we locate the source close to a null point with a reversed-Y shape. The coronal disturbance induced by the flare propagates along the footpoints of a system of loops in a unique domain of connectivity. Those loops exist *before, during and after* the flare period.

ACKNOWLEDGMENTS

This research is funded by the European Commission's Human Potential Programme through the European Solar Magnetism Network (contract HPRN-CT-2002-00313). SOHO is a project of international cooperation between ESA and NASA.

REFERENCES

Amari, T., Aly, J. J., Luciani, J. F., Boulmezaoud, T. Z., Mikic, Z., 1997, Sol. Phys., 174, 129

Amari, T., Boulmezaoud, T. Z., Mikic, Z., 1999, A&A, 350, 1051

Labonte, B. J., Mickey, D. L., Leka, K. D., 1999, Sol. Phys., 189, 1

Lin, H., Kuhn, J.R., Coulter, R., 2004, ApJ 613, L177

Mickey, D. .L., Canfield, R. C., Labonte, B. J., Leka, K. D., Waterson, M. F., Weber, H. M., 1996, Sol. Phys., 168, 229

Régnier, S., Amari, T., Kersalé, E., 2002, A&A, 392, 1119